A Zika virus envelope mutation preceding the 2015 epidemic enhances virulence and fitness for transmission

Chao Shan[a,b,1,2], Hongjie Xia[a,1], Sherry L. Haller[c,d,e], Sasha R. Azar[c,d,e], Yang Liu[a], Jianying Liu[c,d], Antonio E. Muruato[c], Rubing Chen[c,d,e,f], Shannan L. Rossi[c,d,f], Maki Wakamiya[a], Nikos Vasilakis[d,f,g,h,i], Rongjuan Pei[b], Camila R. Fontes-Garfias[a], Sanjay Kumar Singh[j], Xuping Xie[a], Scott C. Weaver[c,d,e,k,l,2], and Pei-Yong Shi[a,d,e,k,l,2]

[a]Department of Biochemistry and Molecular Biology, University of Texas Medical Branch, Galveston, TX 77555; [b]State Key Laboratory of Virology, Wuhan Institute of Virology, Chinese Academy of Sciences, 430071 Wuhan, China; [c]Department of Microbiology and Immunology, University of Texas Medical Branch, Galveston, TX 77555; [d]Institute for Human Infections and Immunity, University of Texas Medical Branch, Galveston, TX 77555; [e]Institute for Translational Science, University of Texas Medical Branch, Galveston, TX 77555; [f]Department of Pathology, University of Texas Medical Branch, Galveston, TX 77555; [g]World Reference Center of Emerging Viruses and Arboviruses, University of Texas Medical Branch, Galveston, TX 77555; [h]Center for Biodefence and Emerging Infectious Diseases, University of Texas Medical Branch, Galveston, TX 77555; [i]Center for Tropical Diseases, University of Texas Medical Branch, Galveston, TX 77555; [j]Department of Neurosurgery-Research, The University of Texas MD Anderson Cancer Center, Houston, TX 77030; [k]Sealy Institute for Vaccine Sciences, University of Texas Medical Branch, Galveston, TX 77555; and [l]Sealy Center for Structural Biology and Molecular Biophysics, University of Texas Medical Branch, Galveston, TX 77555

Edited by Peter Palese, Icahn School of Medicine at Mount Sinai, New York, NY, and approved July 2, 2020 (received for review March 26, 2020)

Arboviruses maintain high mutation rates due to lack of proofreading ability of their viral polymerases, in some cases facilitating adaptive evolution and emergence. Here we show that, just before its 2013 spread to the Americas, Zika virus (ZIKV) underwent an envelope protein V473M substitution (E-V473M) that increased neurovirulence, maternal-to-fetal transmission, and viremia to facilitate urban transmission. A preepidemic Asian ZIKV strain (FSS13025 isolated in Cambodia in 2010) engineered with the V473M substitution significantly increased neurovirulence in neonatal mice and produced higher viral loads in the placenta and fetal heads in pregnant mice. Conversely, an epidemic ZIKV strain (PRVABC59 isolated in Puerto Rico in 2015) engineered with the inverse M473V substitution reversed the pathogenic phenotypes. Although E-V473M did not affect oral infection of *Aedes aegypti* mosquitoes, competition experiments in cynomolgus macaques showed that this mutation increased its fitness for viremia generation, suggesting adaptive evolution for human viremia and hence transmission. Mechanistically, the V473M mutation, located at the second transmembrane helix of the E protein, enhances virion morphogenesis. Overall, our study revealed E-V473M as a critical determinant for enhanced ZIKV virulence, intrauterine transmission during pregnancy, and viremia to facilitate urban transmission.

Zika | envelope | evolution | transmission

After its discovery in 1947 (1), Zika virus (ZIKV) "silently" circulated in Africa and Asia between primates and mosquitoes in forests with no major outbreaks and only 14 documented human infections in 60 y (2). Since 2007, ZIKV strains from an Asian lineage that spread from Africa decades earlier have emerged to cause outbreaks and severe diseases: The first outbreak occurred on Yap Island in 2007, followed by a large outbreak in French Polynesia in 2013–2014, and finally massive epidemics in the Americas from 2015–2016. The most devastating diseases associated with the recent ZIKV epidemics comprise congenital Zika syndrome (CZS) in fetuses of infected pregnant women and Guillain-Barré syndrome in adults (3–5). Like other flaviviruses, the ZIKV genome (Fig. 1*A*) encodes three structural proteins (capsid [C], premembrane/membrane [prM], and envelope [E]) and seven nonstructural proteins (NS1, NS2A, NS2B, NS3, NS4A, NS4B, and NS5). The structural proteins form virions that contain genomic RNA. The nonstructural proteins participate in viral replication, virion assembly, and evasion of host immunity (6, 7). The NS2A protein has recently been shown to orchestrate flavivirus assembly through recruiting structural proteins and viral RNA (8, 9).

One hypothesis for the sudden and dramatic emergence of ZIKV is that genetic changes enhanced transmission and more severe diseases (10). The timing of the massive emergence in 2015 correlates with the acquisition of seven amino acid changes in the Asian lineage ZIKV strains from 2010 to 2013 (Fig. 1 *A* and *B*): C-T106A, prM-V1A, prM-S17N, E-V473M, NS1-A188V, NS5-M114V, and NS5-M872V. Among the seven mutations, two have been functionally analyzed. (1) Mutation NS1-A188V was shown to slightly enhance the infectivity of ZIKV in laboratory *Aedes aegypti* mosquitoes as well as to suppress type I IFN production in mammals (11, 12). (2) Conflicting results were reported for mutation prM-S17N such that when engineered into

Significance

ZIKV has "silently" circulated without causing severe diseases for decades since its discovery in 1947. Our study demonstrated that ZIKV acquired an evolutionary mutation in viral envelope gene (E-V473M) that increases virulence, maternal-to-fetal transmission during pregnancy, and viremia in nonhuman primates to facilitate urban transmission since 2013, which may be responsible for the recent emergence and severe diseases. Our results underscore the potential that high genetic mutation frequencies during arbovirus replication and transmission between mosquito and vertebrate hosts could lead to emergence and reemergence of those pathogens. Understanding the mechanisms of emergence and enhanced transmission is essential to detect and respond to future arbovirus outbreaks.

Author contributions: C.S., H.X., S.L.H., S.R.A., Y.L., S.L.R., N.V., X.X., S.C.W., and P.-Y.S. designed research; C.S., H.X., S.L.H., S.R.A., Y.L., J.L., A.E.M., R.C., S.L.R., M.W., N.V., R.P., C.R.F.-G., S.K.S., and X.X. performed research; C.S., H.X., S.L.H., S.R.A., Y.L., J.L., A.E.M., R.C., S.L.R., M.W., N.V., R.P., C.R.F.-G., S.K.S., X.X., S.C.W., and P.-Y.S. analyzed data; and C.S., H.X., S.L.H., S.R.A., S.C.W., and P.-Y.S. wrote the paper.

The authors declare no competing interest.

This article is a PNAS Direct Submission.

[1]C.S. and H.X. contributed equally to this work.

[2]To whom correspondence may be addressed. Email: shanchao@wh.iov.cn, sweaver@UTMB.edu, or peshi@UTMB.edu.

This article contains supporting information online at https://www.pnas.org/lookup/suppl/doi:10.1073/pnas.2005722117/-/DCSupplemental.

First published August 3, 2020.

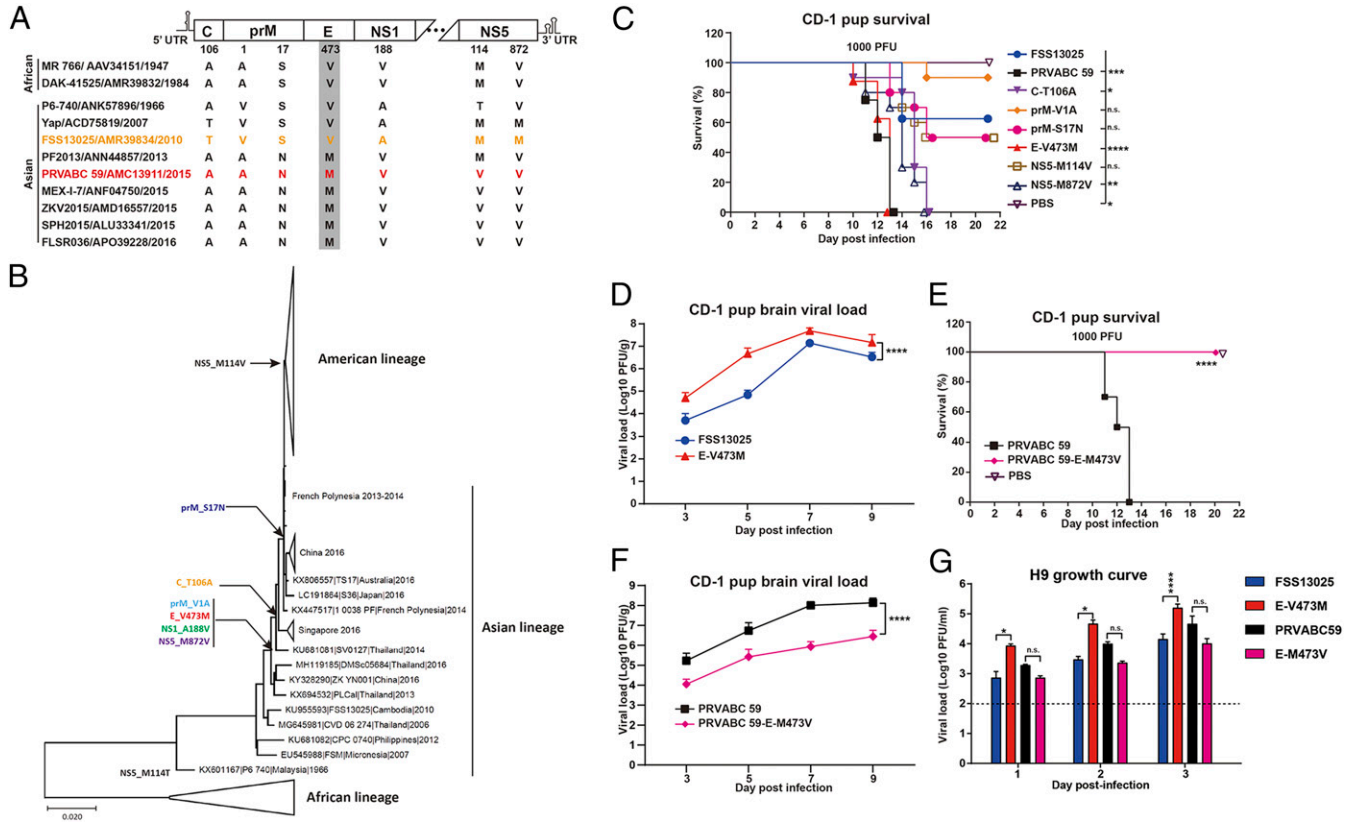

Fig. 1. The effect of E-V473M mutation on neurovirulence. (*A*) Evolutionary mutations among ZIKV strains from the Asian and African lineages. The year of isolation is indicated for each strain. Conserved amino acid changes are labeled using the FSS13025 strain as a reference. Strains FSS13025 and PRVABC59, representing preepidemic and epidemic isolates, are colored in yellow and red, respectively. (*B*) Phylogenetic analysis. Individual mutations from *A* are colored and indicated at branch points of the phylogenetic tree. To construct a phylogenetic tree, the complete open reading frame (ORF) nucleotide sequences of 73 representative ZIKV strains were aligned and analyzed using the maximum likelihood method with 1,000 bootstrap replicates using the MEGA X program. ZIKV strains are labeled by GenBank accession number, followed by strain name, country, and year of collection. (*C*) Neurovirulence of ZIKVs with single amino acid mutation. One-day-old CD-1 pups were infected with 1,000 PFU of FSS13025, C-T106A, prM-V1A, prM-S17N, E-V473M, NS1-A188V, NS5-M114V, or NS5-M872V virus via the intracranial route ($n = 10$ per group). All mutations were engineered into the preepidemic FSS13025 in *SI Appendix*, Fig. S1. The pups were monitored for morbidity and mortality. Survival curves are presented. Epidemic strain PRVABC59 and phosphate buffered saline (PBS) were included as a positive and negative control, respectively. E-V473M, NS5-M872V, and C-T106A mutants exhibited the highest neurovirulence among the tested viruses. Log-rank test was performed for statistical analysis. $^{****}P < 0.0001$, $^{***}P < 0.001$, $^{**}P < 0.01$, $^{*}P < 0.05$, $P > 0.5$ nonsignificant (n.s.). The statistical analysis was performed in reference to FSS13025. (*D*) Brain viral loads from the FSS13025- and E-V473M–infected pups. Pups from *A* were sacrificed and measured for brain viral loads at indicated days postinfection. Two-way ANOVA was performed for statistical analysis. $^{****}P < 0.0001$. (*E*) Neurovirulence of reverse mutation E-M473V in epidemic strain PRVABC59. Log-rank test was performed for statistical analysis. $^{****}P < 0.0001$. (*F*) Brain viral loads from PRVABC59- and E-M473V–infected pups. The experimental procedures in *E* and *F* were identical to *C* and *D*, respectively. Two-way ANOVA was performed for statistical analysis. $^{****}P < 0.0001$. (*G*) Replication kinetics of FSS13025, E-V473M, PRVABC59, and E-M473V on embryonic stem H9 cells. The H9 cells were infected with indicated viruses at an MOI of 0.5. Plaque assay was performed to measure infectious viruses in culture supernatants on day 1–3 postinfection. Asterisks indicate significant differences as analyzed by two-way ANOVA with multiple comparisons. $^{****}P < 0.0001$; $^{*}P < 0.5$ significant; $P > 0.5$ nonsignificant (n.s.). Error bars denote SDs.

the preepidemic strain FSS13025, this mutation increased microcephaly in fetuses following direct injection into the fetal brain (13); however, the reverse mutation prM-N17S in the epidemic strain PRVABC59 did not affect microcephaly or vertical transmission in pregnant mice (14). No studies have addressed the effect of the other five mutations on ZIKV virulence or epidemic potential.

To examine potential virulence effects of these seven mutations, we engineered individual changes into an infectious clone of preepidemic FSS13025 ZIKV (15). Transfection of Vero cells with the mutant viral RNAs generated E protein-positive cells (*SI Appendix*, Fig. S1*A*) and infectious viruses with plaque morphologies similar to the wild-type (WT) FSS13025 (*SI Appendix*, Fig. S1*B*). The recovered mutant viruses were tested for neurovirulence by intracranially infecting 1-d-old CD-1 pups with 1,000 plaque-forming units (PFU) of virus. Compared with the WT FSS13025, mutants C-T106A, E-V473M, and NS5-M872V produced significantly higher mortality rates, with the E-V473M mutant generating a mortality curve equivalent to that of the epidemic strain PRVABC59 (Fig. 1*C*). Notably, mutant prM-S17N, previously reported to be highly neurovirulent (13), only slightly increased the mortality rate (Fig. 1*C*).

Next, we examined the combinatory effect of the three most virulent mutations. Three double mutants (C-T106A+E-V473M, C-T106A+NS5-M872V, and E-V473M+NS5-M872V) and one triple mutant (C-T106A+E-V473M+NS5-M872V) were prepared (*SI Appendix*, Fig. S2*A*). Upon intracranial infection of 1-d-old CD-1 pups, none of the double or triple mutants caused significantly higher mortality rates than the single mutant E-V473M (*SI Appendix*, Fig. S2 *B* and *C*), suggesting that these mutations may have counteractive rather than additive effects. Since the single mutant E-V473M consistently exhibited the

highest neurovirulence among all tested variants (Fig. 1*C* and *SI Appendix*, Fig. S2), we decided to further characterize this mutation.

In agreement with higher mortality of E-V473M in CD-1 pups infected with 100 (*SI Appendix*, Fig. S3) or 1,000 PFU (Fig. 1*C*), significantly higher viral loads were detected in the brains of E-V473M–infected mice compared to the FSS13025-infected animals (Fig. 1*D*). To verify these results, we engineered a reverse mutation E-M473V into epidemic strain PRVABC59 (*SI Appendix*, Fig. S1). No mortality was observed when pups were intracranially infected with 100 (*SI Appendix*, Fig. S3) or 1,000 PFU (Fig. 1*E*) of E-M473V virus, whereas all animals succumbed to PRVABC59 infection. Congruently, the E-M473V virus produced lower viral loads in the brains than PRVABC59 (Fig. 1*F*). In line with the in vivo results, in H9 embryonic neural stem cells, E-V473M virus produced 10-fold more infectious virus than FSS13025, whereas the reverse mutant E-M473V generated threefold less virus than PRVABC59 (Fig. 1*G*). The results demonstrate that E-V473M increases the neurovirulence of preepidemic Asian lineage ZIKV.

We examined the effect of the E-V473M mutation on ZIKV replication in an A129 mouse (*IFNAR1*$^{-/-}$) model (16). Three-week-old A129 mice were s.c. infected with 10 PFU of two pairs of ZIKVs: WT versus E-V473M FSS13025, or WT versus E-M473V PRVABC59 (Fig. 2*A*). On day 4 postinfection, mean peak E-V473M viremia was 1,000-fold higher than FSS13025 viremia, whereas the mean E-M473V viremia was 50-fold lower than PRVABC59 viremia (Fig. 2*B*). The viremia differences

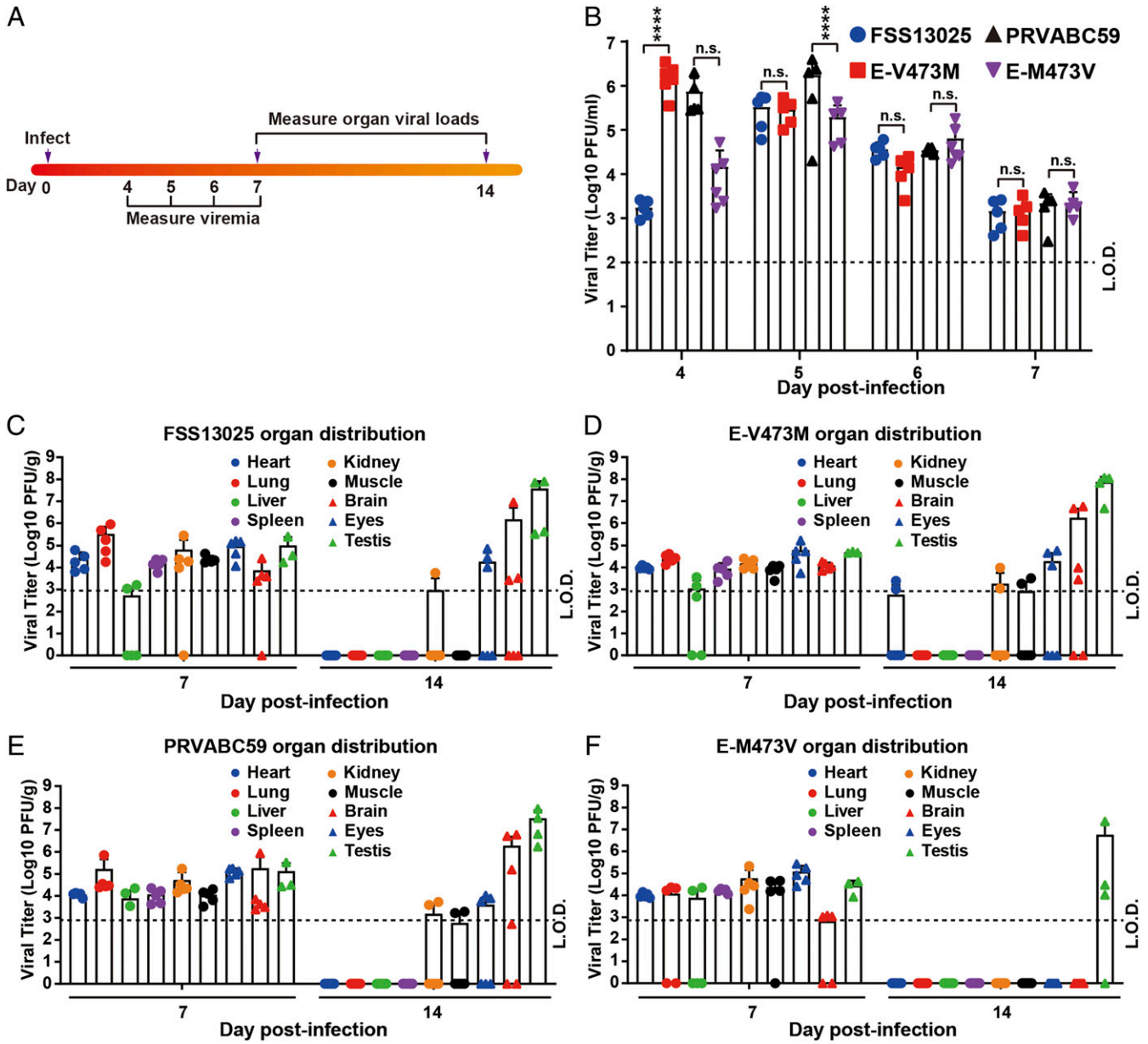

Fig. 2. Comparison of organ viral loads from A129 mice infected with FSS13025, E-V473M, PRVABC59, or E-M473V virus. (*A*) Experimental scheme. Three-week-old A129 mice were infected with 10 PFU of FSS13025, E-V473M, PRVABC59, or E-M473V ($n = 5$–6 per group). (*B*) Viremia. Viremia at day 4–7 was measured using plaque assay. Two-way ANOVA was performed for statistical analysis. ****$P < 0.0001$; $P > 0.5$ nonsignificant (n.s.). (*C*–*F*) Organ viral loads. At day 7 and 14 postinfection, the animals were sacrificed and measured for organ viral loads using plaque assay. The organ viral loads are presented for animals infected with FSS13025 (*C*), E-V473M (*D*), PRVABC59 (*E*), or (*F*) E-M473V virus. Nine different organs were analyzed and presented in different colors. The numbers of testes are in the range of 3–4. Error bars denote SD. L.O.D., limit of detection.

gradually disappeared from day 5–7 (Fig. 2*B*). On day 7 postinfection, infectious ZIKV was detected in all organs (Fig. 2 *C*–*F*). On day 14 postinfection, infectious viruses were cleared from some organs; however, more organs retained viruses in the E-V473M– and PRVABC59-infected mice than the FSS13025- and E-M473V–infected animals (Fig. 2 *C*–*F*). In addition, when male A129 mice were s.c. infected with 10 PFU of virus, total and motile sperm counts were lower in the E-V473M and PRVABC59 groups than the FSS13025 and E-M473V groups, on day 14 postinfection (Fig. 3). These results indicate that E-V473M and PRVABC59 yield higher viral titers in multiple organs when compared to the preepidemic FSS13025 virus and to the less pathogenic E-M473V virus.

Since CZS represents the most devastating outcome of ZIKV infection, we characterized the impact of E-V473M on maternal-to-fetal transmission in a murine pregnancy model (Fig. 4*A*) (17). Nine- to ten-week-old C57BL/6J female mice were mated and closely monitored for vaginal plugs (defined as embryonic day 0.5 [E0.5]). At E5.5, anti-IFNAR1 antibodies were intraperitoneally administered to the animals to facilitate ZIKV infection. At E6.5, the pregnant mice were s.c. infected with 10^3 PFU of FSS13025, E-V473M, PRVABC59, or E-M473V virus. At E13.5, the animals were sacrificed and viral loads quantified in maternal and fetal organs (Fig. 4*A*). No significant differences in viral loads were observed in maternal spleens or brains between the FSS13025 and E-V473M infections (Fig. 4 *B* and *C*) or between the PRVABC59 and E-M374V (Fig. 4 *F* and *G*). However, significantly higher viral loads in the placenta (Fig. 4 *D* and *H*) and fetal brain (Fig. 4 *E* and *I*) were detected from the E-V473M and PRVABC59 infections than the FSS13025 and E-M473V infections; the differences were in the range of two to four folds. Corroborating the in vivo results, infections of human trophoblast HTR-8 cells with E-V473M and PRVABC59 produced significantly higher titers than the corresponding FSS13025 and E-M473V (Fig. 4*J*). These results indicate that mutation E-V473M increases the potential for maternal-to-fetal transmission during pregnancy.

To examine potential effects on transmission efficiency, we compared E-V473M to parental FSS13025 for oral infection of *Aedes aegypti*, the main ZIKV vector in the Americas (18). Mosquitoes derived from Galveston, Texas, were fed on artificial blood meals containing 10^6 PFU/mL of E-V473M or FSS13025 virus. Engorged mosquitoes were incubated and assayed for viral RNA on day 14 postfeeding. Similar to previous findings (15, 19), FSS13025 and E-V473M viruses generated similar infection rates of 57% and 55%, respectively (Fig. 5). These results suggest that mutation E-V473M does not affect ZIKV infection of the epidemic vector.

To determine if E-V473M might enhance epidemic transmission by enhancing human viremia, which would lead to more efficient infection of mosquito vectors, we infected cynomolgus macaques to determine its effect on viremia (Fig. 6*A*). We took a competition fitness approach to directly compare the replication efficiencies of FSS13025 and E-V473M viruses in the same host. This method is highly sensitive and well controlled because the two viruses replicate in the same host environment; it also reduces animal usage compared to individual viruses used to infect large cohorts. Equal PFU amounts of FSS13025 and E-V473M viruses (10^4 PFU each) were mixed, and an approximately equal viral RNA ratio was confirmed by pyrosequencing the E-V473M single nucleotide polymorphisms (SNP) in RT-PCR amplicons. After s.c. infection with the virus mixture, all three monkeys developed detectable infectious viremia ($\leq 10^3$ PFU/mL) with one animal having viremia up to 10 d postinfection (*SI Appendix*, Fig. S4). Blood samples were collected on days 1–4 (Fig. 6 *B*–*D*), and the ratios of FSS13025 to E-V473M viruses were estimated by RT-PCR amplification of a genome region surrounding the SNP, followed by pyrosequencing. The E-V473M virus consistently won the competition except at one early timepoint (day 1 in animal 142590) and one late timepoint (day 4 in animal 13424; Fig. 6 *E*–*G*). Overall, these results suggest that the E-V473M mutation confers an advantage to the preepidemic FSS13025 for viremia generation in a nonhuman primate model of human infection, which is key to infection of mosquito vectors. However, due to the small number of animals in the experiment, more studies are needed to confirm the observation.

Finally, we analyzed the mechanism of E-V473M in enhancing ZIKV replication in mammalian hosts. E-V473M is located in the second transmembrane helix of E protein (Fig. 7*A*) (20, 21). When BHK-21 cells were infected with E-V473M and FSS13025 viruses (multiplicity of infection [MOI] of 1), comparable viral RNA levels were detected at 1–7 h postinfection (*SI Appendix*, Fig. S5), suggesting that both viruses bind and enter cells at similar efficiencies. At 14–48 h postinfection (Fig. 7*B*), similar intracellular viral RNA levels were detected for both viruses, suggesting that E-V473M does not affect viral RNA synthesis (Fig. 7*C*). Notably, at 20–48 h postinfection, the E-V473M virus

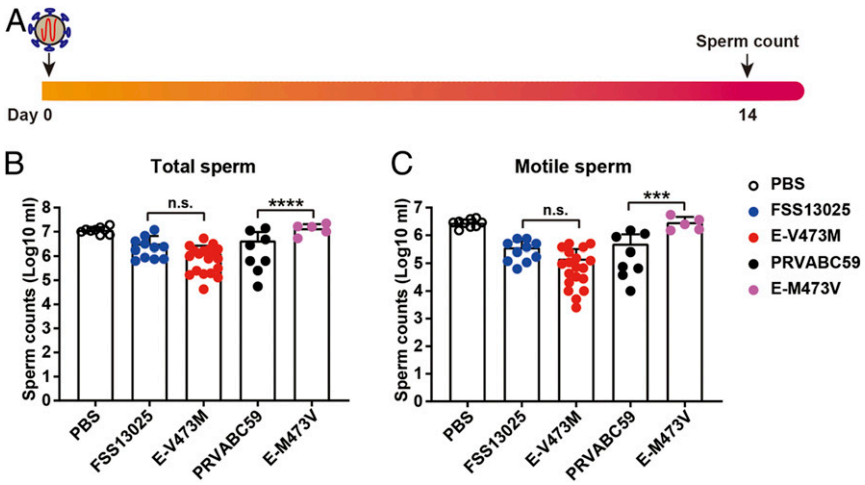

Fig. 3. Sperm count analysis of A129 mice infected with FSS13025, E-V473M, PRVABC59, or E-M473V ZIKV strains. (*A*) Experimental scheme. Three-week-old male A129 was infected with 10 PFU of FSS13025, E-V473M, PRVABC59, or E-M473V virus. At day 14 postinfection, total sperm counts (*B*) and motile sperm counts (*C*) were measured. PBS was included as a negative control. Error bars denote SD. Two-way ANOVA was performed for statistical analysis. ***$P < 0.001$; ****$P < 0.0001$; $P > 0.5$ nonsignificant (n.s.).

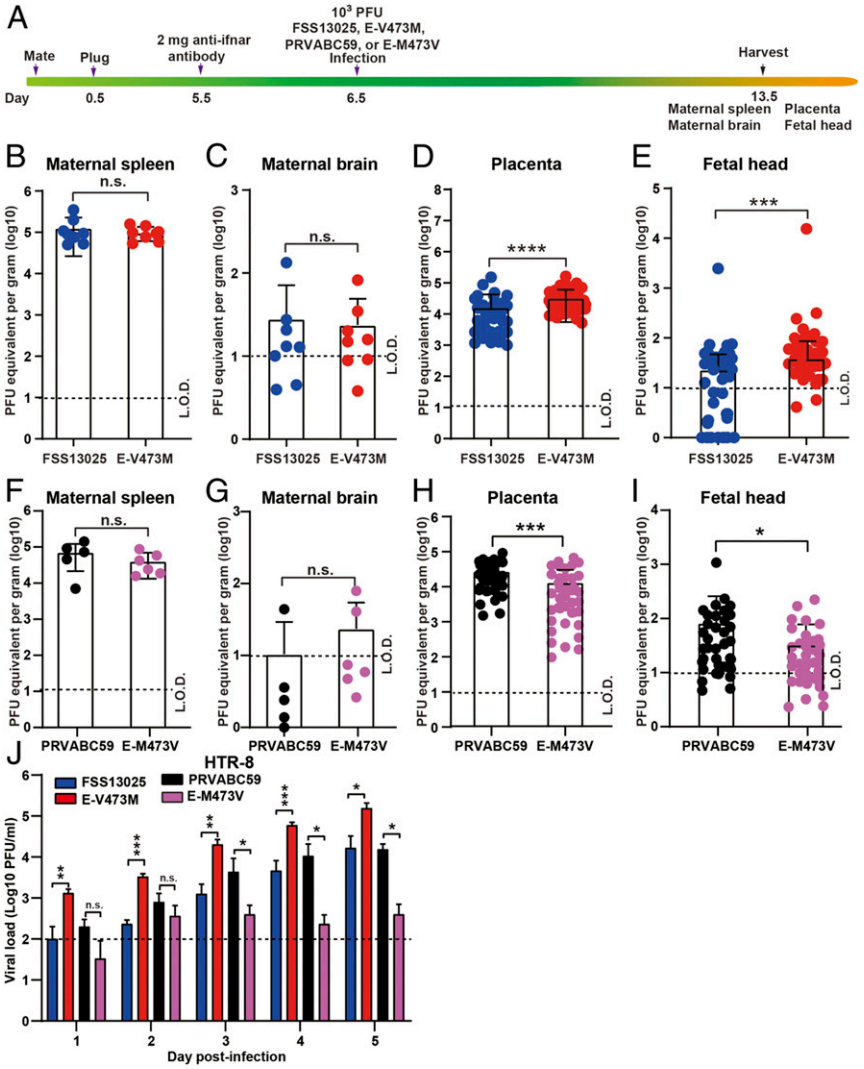

Fig. 4. The effect of E-V473M mutation on intrauterine ZIKV transmission in pregnant mice. (*A*) Experimental scheme. Nine- to ten-week-old female C57BL/6J mice (n = 5–8) were mated with nine-week-old male C57BL/6J mice. Once vaginal plugs were identified, the mice were defined as embryotic stage 0.5 (E0.5). At E5.5, the animals were intraperitoneally administered with 2 mg of anti-IFNAR1 antibody (MAR1-5A3). At E6.5, the mice were infected with 10^3 PFU of FSS13025, E-V473M, PRVABC59, or E-M473V virus via the s.c. route at footpads. At E13.5, maternal and fetal tissues were harvested and quantified for viral loads using quantitative RT-PCR. Viral loads are presented for maternal spleen (*B* and *F*), maternal brain (*C* and *G*), placenta (*D* and *H*), and fetal head (*E* and *I*). Experiments *B* to *E* used 8 pregnant mice and >40 fetuses. Experiments *F* to *I* used 5–6 pregnant mice and >40 fetuses. (*J*) Growth kinetics of FSS13025, E-V473M, PRVABC59, and E-M473V on trophoblast HTR-8 cells. HTR-8 cells were infected with the indicated viruses at an MOI of 0.01. Plaque assay was performed to measure infectious viruses in culture supernatants on day 1–5 postinfection. Asterisks indicate significant differences as analyzed by Mann-Whitney test (*B–I*) or Student's *t* test (*J*). ****$P < 0.0001$; ***$P < 0.001$; ** $P < 0.01$; *$P < 0.5$ significant; $P > 0.5$ nonsignificant (n.s.). Error bars denote SDs.

produced significantly more extracellular viral RNA (Fig. 7*D*), intracellular infectious virus (Fig. 7*E*), and extracellular infectious virus (Fig. 7*F*) than FSS13025 virus, suggesting that mutation E-V473M enhances virion assembly. Corroborating the infection results, transient expression of viral prM-E alone produced equal levels of intracellular prM and E proteins in BHK-21 and 293T cells (Fig. 7*G*); however, the E-V473M mutant prM-E plasmid secreted 1.5- to 2.8-fold more extracellular prM and E proteins than the WT construct (Fig. 7*H*), suggesting that E-V473M enhances virus-like particle production. Collectively, these results indicate that E-V473M increases viral replication through promoting virion morphogenesis.

Overall, our study revealed that the E-V473M substitution, which preceded the American epidemic, enhances ZIKV replication, leading to increased neurovirulence, maternal-to-fetal transmission during pregnancy, and viremia in mouse and nonhuman primate models. A higher viremia conferred by the E-V473M substitution may translate into greater peripheral viremia and more efficient infection of the mosquito vector upon blood feeding. The genetic changes reported here, together with naive herd immunity (22), heterologous flavivirus preimmunity (23–27), environmental factors (28), and genetic predisposition (29), may have led to the recent emergence and severe diseases (30, 31). There are more than 500 known arboviruses of which ~100 are capable of causing disease in humans (32). Due to the high mutation frequencies of viral RNA-dependent RNA polymerases and the transmission cycle between mosquito and vertebrate hosts, arboviruses will continue to emerge and reemerge. Understanding the mechanisms of emergence and enhanced transmission and spread, combined with improved surveillance to identify such changes, is essential to detect and respond to future arbovirus outbreaks.

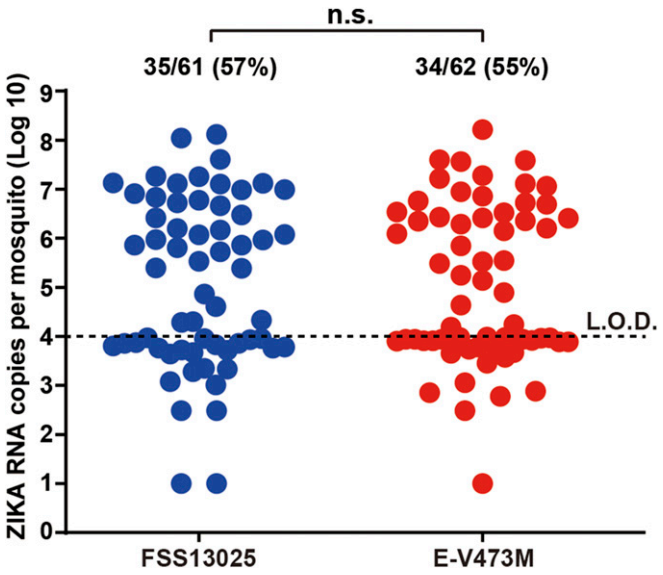

Fig. 5. Comparison of oral infectivity of WT FSS13025 and E-V473M ZIKVs in *A. aegypti* mosquitoes. Artificial blood meal was prepared by mixing human blood cells with FSS13025 or E-V473M virus to final concentrations of 10^6 PFU/mL. Engorged mosquitoes were reared for 14 d and quantified for viral RNAs using quantitative RT-PCR. The statistical difference was analyzed by Mann-Whitney test. $P > 0.5$ nonsignificant (n.s.).

Materials and Methods

Ethics Statement. Mouse studies were performed in accordance with the recommendations in the Guide for the Care and Use of Laboratory Animals (33). The protocol was approved by the Institutional Animal Care and Use Committee at UTMB (Protocol numbers 1708051 and 1609041).

Mice were nonspecifically and blindly distributed into their respective cohorts, but sample collection and analyses were not blinded. s.c. and i.p. injections were performed under anesthesia that was induced and maintained with isoflurane. All efforts were made to minimize animal suffering.

For cynomolgus macaque (*Macaca fascicularis*) studies, healthy adolescent (2- to 5-y-old) animals of Chinese origin were utilized. All animals were seronegative for herpes B virus, simian immunodeficiency virus, simian retrovirus, and simian T-lymphotropic virus. Additional hemagglutinin inhibition testing revealed no previous flavivirus (ZIKV, WNV, yellow fever [YFV], St. Louis encephalitis [SLEV], DENV-1-4) or alphavirus (chikungunya [CHIKV]; Venezuelan [VEEV], eastern [EEEV], or western equine encephalitis [WEEV]; Sindbis [SINV], or Semliki forest virus [SFV]) exposure. Prior to ZIKV infection (≥6 mo), these animals were exposed to CHIKV vaccines or sham-vaccinated and challenged with WT CHIKV (34). Animals were individually housed in steel caging (Allentown. Inc.) with free access to water. Commercial chow was provided twice daily, and supplementation was provided daily or at the discretion of the veterinary staff. Health checks were performed twice daily from the date of infection until the end of the study. Procedures and manipulations were conducted with care to minimize any potential distress, pain, or discomfort by trained veterinary and/or research staff.

Following overnight fasts, macaques were anesthetized by intramuscular injection with ketamine (5–20 mg/kg), then weighed. Blood was collected by venipuncture into K_2EDTA or serum separator vacutainer tubes (Beckton Dickinson).

Phylogenetic Analysis of Zika Virus. To construct a phylogenetic tree, the complete ORF nucleotide sequences of 73 representative ZIKV strains were aligned and analyzed using the maximum likelihood method with 1,000 bootstrap replicates using the MEGA X program. ZIKV strains are labeled by GenBank accession number, followed by strain name, country, and year of collection.

Neurovirulence on Newborn CD-1 Mice. Groups of 1-d-old outbred CD-1 mice (n = 10) were injected intracranially (I.C.) with WT or mutants virus at a dose of 1,000 PFU or 100 PFU. Mice were monitored daily for morbidity and mortality (35).

Viral Load in Brain of CD-1 Mice. Groups of 1-d-old outbred CD-1 mice (n = 10–14) were injected I.C. with 1,000 PFU of FSS13025 WT, E-V473M, PRVABC59, or E-M473V virus. The mice brains were harvested at day 3, 5, 7, and 9 postinfection into 2-mL Eppendorf tubes containing 0.5 mL DMEM with a bead. The tissues were homogenized by Qiagen TissueLyser II. After centrifugation at 15,000 rpm for 5 min, the supernatants were used for plaque assay to measure the viral loads.

Mouse Pregnancy Study. C57BL/6J mice were purchased from the Jackson Laboratory. Nine- to ten-week-old female C57BL/6J mice were paired with nine-week-old male mice (36). The vaginal plug was checked daily. Once the plug was identified, the mice were defined at starting embryotic stage (E0.5). At embryonic day E5.5, pregnant dams were treated with 2 mg injection of anti-IFNAR1 antibody. At E6.5, mice were inoculated with 10^3 PFU of FSS13025 WT, E-V473M, PRVABC59, or E-M473V by s.c. injection in the footpad. All animals were sacrificed at E13.5, and fetuses, placentas, and maternal tissues were harvested. Organs were weighed and homogenized using a Qiagen TissueLyser II, and serum was prepared after coagulation and centrifugation. Tissue samples and serum from ZIKV-infected mice were extracted with the RNeasy Mini Kit (Qiagen). ZIKV RNA levels were determined

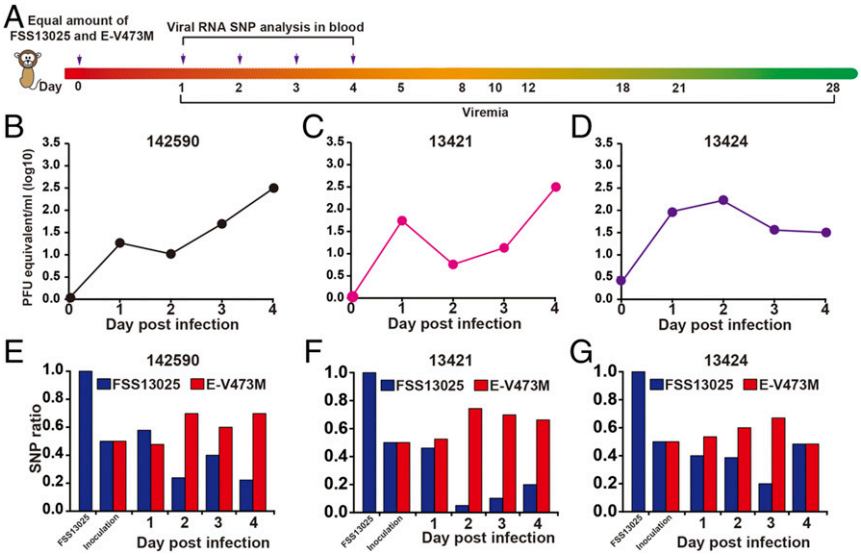

Fig. 6. Competition of FSS13025 and E-V473M viruses in nonhuman primates. (*A*) Experimental scheme. Three cynomolgus monkeys were s.c. infected with a mixture of equal amounts (10^4 PFU) of FSS13025 and E-V473M viruses. Viremias of individual monkeys were measured by quantitative RT-PCR (*B–D*). The ratios of FSS13025:E-V473M viruses in the inoculum and day 1–4 blood samples were quantified by pyrosequencing (*E–G*). The pyrosequencing SNP results indicate the outcome of the competitions.

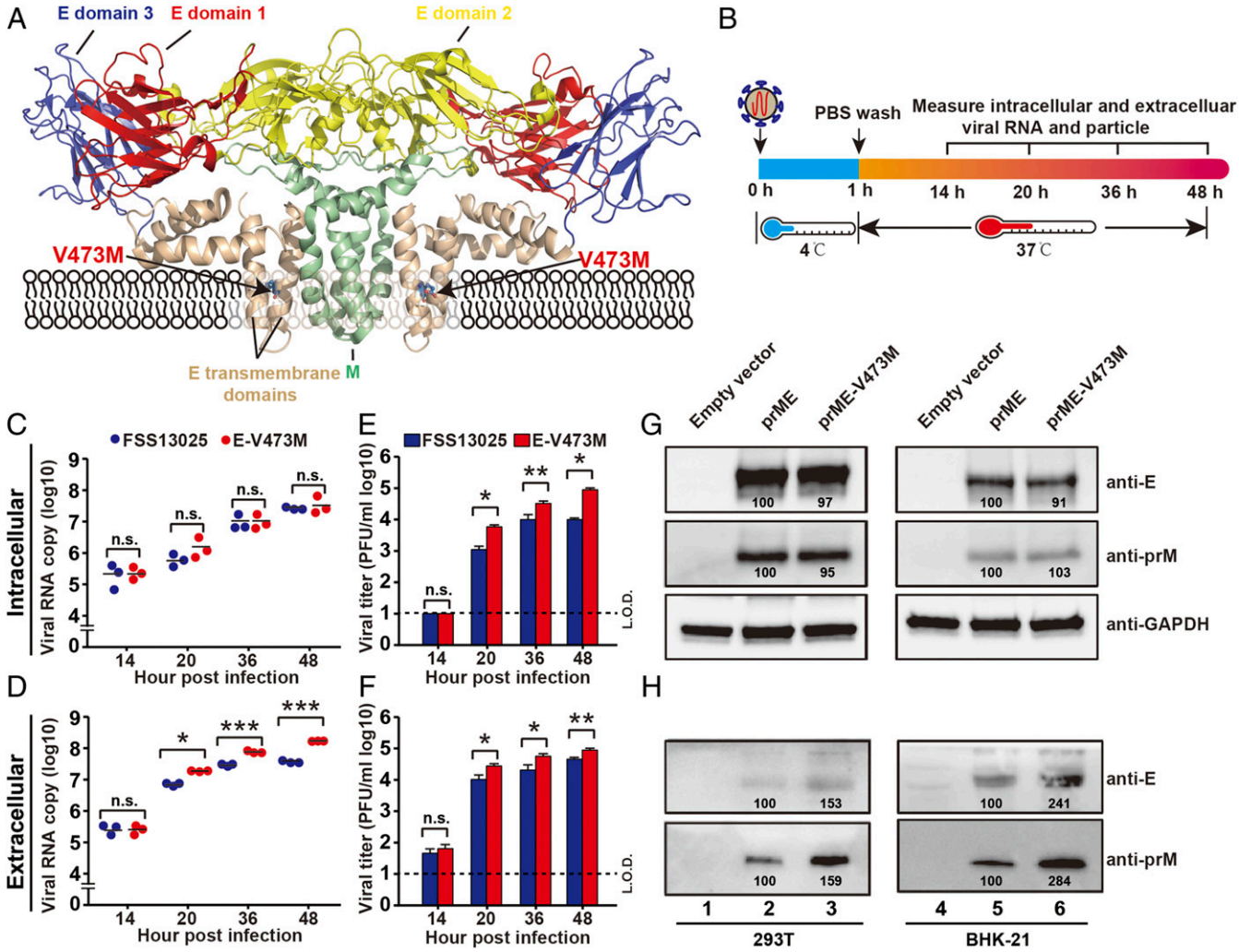

Fig. 7. The effect of E-V473M mutation on ZIKV infection cycle. (*A*) Three-dimensional structures of ZIKV E and M proteins. Substitution V473M is located in the second transmembrane helix of E protein. Three subdomains of the E protein and mature M protein are indicated. (*B*) Experiment scheme. BHK-21 cells were incubated with FSS13025 or E-V473M virus (MOI of 1 PFU/cell) at 4 °C. After 1 h incubation, virus inocula were removed, and cells were washed three times with PBS. The cells were then incubated at 37 °C. At 14, 20, 36, and 48 h postinfection, the infected cells were quantified for intracellular viral RNA (*C*), extracellular viral RNA (*D*), intracellular virus (*E*), and extracellular virus (*F*). Intracellular viral RNAs were measured by quantitative RT-PCR and normalized using cellular GAPDH RNA. Infectious viruses were measured by plaque assay. (*G* and *H*) The effect of the E-V473M substitution on empty virus-like particle (VLP) production. WT or E-V473M prM-E genes were transiently expressed from plasmid pXJ in 293T or BHK-21 cells. Equal amounts of plasmids (1 μg) were transfected into cells using X-tremeGENE 9 DNA transfection reagent. At 48 h posttransfection, the intracellular and extracellular levels of E and prM proteins were analyzed by Western blotting. The relative protein amounts were quantified by Image J and indicated below individual bands. The expression levels of WT prM-E were set as 100. Statistical values were analyzed by unpaired Student's *t* test (*D*–*F*). $P > 0.5$ nonsignificant (n.s.), $^{*}P < 0.05$, $^{**}P < 0.01$, $^{***}P < 0.001$. Error bars denote SDs.

by TaqMan one-step qRT-PCR on LightCycler 480 System (Roche). Viral burden is expressed on a $\log_{10}$ scale as viral RNA equivalents per gram after comparison with a standard curve produced using serial 10-fold dilutions of ZIKV RNA from known quantities of infectious virus. For ZIKV, the following primer/probe sets were used: forward primer (1183F: 5′-CCACCAATGTTCTCTTGCAGACATATTG-3′), reverse primer (1268R: 5′-TTCGGACAGCCGTTGTCCAACACAAG-3′), and probe (1213F: 5′-56-FAM/AGCCTACCT TGACAAGCAGTC/3IABkFQ-3′) (37).

Data Analysis. All data were analyzed with GraphPad Prism v7.02 software. Data are expressed as the mean ± SD. Comparisons of groups were performed using Mann-Whitney test, Student's *t* test, or two-way ANOVA with a multiple comparison's correction. A *P* value of <0.05 indicates statistically significant.

Data Availability. Source data for generating main figures are available in the *SI Appendix*.

ACKNOWLEDGMENTS. We thank Michael S. Diamond, Gong Cheng, and Cheng-Feng Qin for helpful discussions and support during the course of the work. P.-Y.S. was supported by NIH Grants AI142759, AI134907, AI145617, and UL1TR001439 and awards from the Sealy & Smith Foundation, Kleberg Foundation, John S. Dunn Foundation, Amon G. Carter Foundation, Gillson Longenbaugh Foundation, and Summerfield Robert Foundation. This research was also supported by NIH Grant AI120942 and the Western Gulf Center of Excellence for Vector-Borne Diseases (Centers for Disease Control and Prevention Grant U01CK000512) to S.C.W.

1. G. W. Dick, S. F. Kitchen, A. J. Haddow, Zika virus. I. Isolations and serological specificity. *Trans. R. Soc. Trop. Med. Hyg.* **46**, 509–520 (1952).
2. D. Musso, D. J. Gubler, Zika virus. *Clin. Microbiol. Rev.* **29**, 487–524 (2016).
3. S. A. Rasmussen, D. J. Jamieson, M. A. Honein, L. R. Petersen, Zika virus and birth defects—Reviewing the evidence for causality. *N. Engl. J. Med.* **374**, 1981–1987 (2016).
4. P. Brasil *et al.*, Zika virus infection in pregnant women in Rio de Janeiro. *N. Engl. J. Med.* **375**, 2321–2334 (2016).
5. V. M. Cao-Lormeau *et al.*, Guillain-Barré syndrome outbreak associated with Zika virus infection in French Polynesia: A case-control study. *Lancet* **387**, 1531–1539 (2016).

6. T. C. Pierson, M. S. Diamond, "Flaviviruses" in *Fields Virology*, D. M. Knipe, P. M. Howley, Eds. (Lippincott Williams & Wilkins, ed. 6, 2013), Vol. vol. 1, pp. 747–794.
7. C. L. Murray, C. T. Jones, C. M. Rice, Architects of assembly: Roles of flaviviridae nonstructural proteins in virion morphogenesis. *Nat. Rev. Microbiol.* **6**, 699–708 (2008).
8. X. Zhang *et al*., Zika virus NS2A-mediated virion assembly. *MBio* **10**, e02375-19 (2019).
9. X. Xie *et al*., Dengue NS2A protein orchestrates virus assembly. *Cell Host Microbe* **26**, 606–622.e8 (2019).
10. J. H. Pettersson *et al*., How did Zika virus emerge in the Pacific Islands and Latin America? *MBio* **7**, e01239-16 (2016).
11. H. Xia *et al*., An evolutionary NS1 mutation enhances Zika virus evasion of host interferon induction. *Nat. Commun.* **9**, 414–427 (2018).
12. Y. Liu *et al*., Evolutionary enhancement of Zika virus infectivity in *Aedes aegypti* mosquitoes. *Nature* **545**, 482–486 (2017).
13. L. Yuan *et al*., A single mutation in the prM protein of Zika virus contributes to fetal microcephaly. *Science* **358**, 933–936 (2017).
14. A. S. Jaeger *et al*., Zika viruses of African and Asian lineages cause fetal harm in a mouse model of vertical transmission. *PLoS Negl. Trop. Dis.* **13**, e0007343 (2019).
15. C. Shan *et al*., An infectious cDNA clone of Zika virus to study viral virulence, mosquito transmission, and antiviral inhibitors. *Cell Host Microbe* **19**, 891–900 (2016).
16. S. L. Rossi *et al*., Characterization of a novel murine model to study Zika virus. *Am. J. Trop. Med. Hyg.* **94**, 1362–1369 (2016).
17. H. M. Lazear *et al*., A mouse model of Zika virus pathogenesis. *Cell Host Microbe* **19**, 720–730 (2016).
18. S. R. Azar, E. E. Diaz-Gonzalez, R. Danis-Lonzano, I. Fernandez-Salas, S. C. Weaver, Naturally infected *Aedes aegypti* collected during a Zika virus outbreak have viral titres consistent with transmission. *Emerg. Microbes Infect.* **8**, 242–244 (2019).
19. C. R. Fontes-Garfias *et al*., Functional analysis of glycosylation of Zika virus envelope protein. *Cell Rep.* **21**, 1180–1190 (2017).
20. D. Sirohi *et al*., The 3.8 Å resolution cryo-EM structure of Zika virus. *Science* **352**, 467–470 (2016).
21. V. A. Kostyuchenko *et al*., Structure of the thermally stable Zika virus. *Nature* **533**, 425–428 (2016).
22. J. V. J. Silva, T. R. R. Lopes, E. F. Oliveira-Filho, R. A. D. S. Oliveira, L. H. V. G. Gil, Perspectives on the Zika outbreak: Herd immunity, antibody-dependent enhancement and vaccine. *Rev. Inst. Med. Trop. São Paulo* **59**, e21 (2017).
23. M. G. Zimmerman *et al*., Cross-reactive Dengue virus antibodies augment Zika virus infection of human placental macrophages. *Cell Host Microbe* **24**, 731–742.e6 (2018).
24. V. N. Camargos *et al*., In-depth characterization of congenital Zika syndrome in immunocompetent mice: Antibody-dependent enhancement and an antiviral peptide therapy. *EBioMedicine* **44**, 516–529 (2019).
25. J. A. Brown *et al*., Dengue virus immunity increases Zika virus-induced damage during pregnancy. *Immunity* **50**, 751–762.e5 (2019).
26. A. M. Fowler *et al*., Maternally acquired Zika antibodies enhance Dengue disease severity in mice. *Cell Host Microbe* **24**, 743–750.e5 (2018).
27. S. V. Bardina *et al*., Enhancement of Zika virus pathogenesis by preexisting antiflavivirus immunity. *Science* **356**, 175–180 (2017).
28. L. R. Petersen, D. J. Jamieson, M. A. Honein, Zika virus. *N. Engl. J. Med.* **375**, 294–295 (2016).
29. L. C. Caires-Júnior *et al*., Discordant congenital Zika syndrome twins show differential in vitro viral susceptibility of neural progenitor cells. *Nat. Commun.* **9**, 475–486 (2018).
30. S. C. Weaver, Emergence of epidemic Zika virus transmission and congenital Zika syndrome: Are recently evolved traits to blame? *MBio* **8**, e02063-16 (2017).
31. H. Xia, X. Xie, C. Shan, P. Y. Shi, Potential mechanisms for enhanced Zika epidemic and disease. *ACS Infect. Dis.* **4**, 656–659 (2018).
32. S. C. Weaver, W. K. Reisen, Present and future arboviral threats. *Antiviral Res.* **85**, 328–345 (2010).
33. National Research Council of the National Academies, *Guide for the Care and Use of Laboratory Animals*, (The National Academies Press, Washington, DC, 8th Ed., 2011).
34. S. L. Rossi *et al*., Immunogenicity and efficacy of a measles virus-vectored chikungunya vaccine in nonhuman primates. *J. Infect. Dis.* **220**, 735–742 (2019).
35. C. Shan *et al*., A live-attenuated Zika virus vaccine candidate induces sterilizing immunity in mouse models. *Nat. Med.* **23**, 763–767 (2017).
36. J. M. Richner *et al*., Vaccine mediated protection against Zika virus-induced congenital disease. *Cell* **170**, 273–283.e12 (2017).
37. Y. Yang *et al*., A cDNA clone-launched platform for high-yield production of inactivated Zika vaccine. *EBioMedicine* **17**, 145–156 (2017).